# Hydrogen-Bond-Assisted Organocatalytic Acetalization of Secondary Alcohols: Experimental and Theoretical Studies

**ARTICLE** *in* THE JOURNAL OF PHYSICAL CHEMISTRY A · APRIL 2015

Impact Factor: 2.69 · DOI: 10.1021/acs.jpca.5b02102 · Source: PubMed



**3 AUTHORS**, INCLUDING:

N. S. Sitnikov

University of Cologne

**17** PUBLICATIONS **46** CITATIONS

SEE PROFILE

Nikolay Viktorovich Somov

Nizhny Novgorod State University

**89** PUBLICATIONS **118** CITATIONS

SEE PROFILE

THE JOURNAL OF PHYSICAL CHEMISTRY A

Article

pubs.acs.org/JPCA

# Hydrogen-Bond-Assisted Organocatalytic Acetalization of Secondary Alcohols: Experimental and Theoretical Studies

Misha Rumyantsev,*[,†,‡] Nikolay S. Sitnikov,[‡] and Nikolay V. Somov[‡]

[†]Nizhny Novgorod State Technical University n.a. R.E. Alekseev, 24 minin st., Nizhny Novgorod 603950, Russia

[‡]Lobachevsky State University of Nizhni Novgorod, 23 Prospekt Gagarina (Gagarin Avenue), Nizhny Novgorod 603950, Russia

Supporting Information

**ABSTRACT:** An efficient method was developed for the acetalization of secondary alcohols in the presence of simple protic pyridinium salts. Direct correlations between the structure and activity of the synthesized catalysts were described. Stabilization via hydrogen bonding of the hemiacetal intermediate by the pyridine derivatives, along with an appropriate increase in the reaction rate, was revealed. The nature of the observed experimental acceleration of the examined reactions catalyzed by pyridinium salts comprising electron-withdrawing groups at certain positions of the pyridinium ring was studied. In this vein, the interpretation of the hydrogen-bonded pretransition-state complexes and transition-state complexes with strong catalysts was also discussed in terms of partial proton transfer. It was concluded that optimized pretransition-state complexes of the catalyst and reactant are useful for the prediction of catalyst efficiency prior to the experiment.

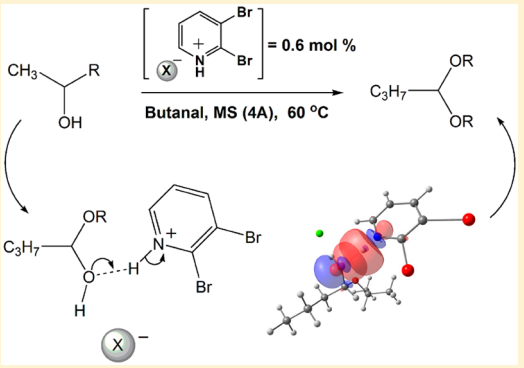


## INTRODUCTION

One of the most common transformations in organic chemistry involves the condensation of carbonyl compounds with alcohols; this is known as acetalization that is usually conducted under acidic conditions.[1−5] The resulting acetals are important moieties in products such as steroids and pharmaceuticals.[6−8] Recently, various studies have reported the significance of cyclic acetals such as 1,3-dioxanes in treating cancer, inflammation, and reperfusion.[9−11] Acetalization is often used in a multistep synthesis when a carbonyl group needs to be protected.[12] This reaction is known to be thermodynamically unfavorable and reversible.[13] The latter characteristic is particularly applicable to the open-chain acetals (acyclic acetals) that have received special attention due to their lability, as compared to cyclic *O,O*-acetals, making them useful in multistep synthesis (e.g., when one needs to cleave an acetal under mild conditions). However, the targeted synthesis of the acyclic acetals from secondary alcohols is rarely reported,[13−16] even though these substrates are useful in organic synthesis because they offer alternative reactivity to the commonly used methanol or ethanol derivatives. Acyclic acetals derived from secondary alcohols can be used in tandem with methyl acetals for the selective protection and deprotection of a carbonyl group in the presence of the other carbonyl-containing functionality.

The rate-determining step in acetalization involves the stabilization and subsequent transformation of a hemiacetal,[17−19] which is quite unstable and easily decomposes back to the alcohol and carbonyl compound. In our opinion, the success of the reaction depends on the ability of the (co)catalyst to interact with the functional groups of hemiacetal and thus increase the stability and reactivity of this intermediate. In general, the utilization of artificial enzymes,[20,21] chemzymes,[22−25] and organic catalysts[13,26−30] seems to be effective for this purpose. Enzymelike small-molecular-weight organocatalysts play an ever increasing role in modern organic synthesis according to the green chemistry concepts. However, the development in this area, the design and targeted synthesis of such catalysts for common organic reactions, is far from complete. Previously, several studies focused on this goal, and consequently, mild and even acid-free organocatalytic acetalization methods were developed.[13,31,32] However, despite the importance of these studies, researchers mainly focused on reactions involving primary alcohols and very little information was given regarding the rates of such reactions or their reactivity compared to routinely employed acids such as HCl and *p*-toluenesulfonic acid (PTSA). Therefore, our primary strategy was to synthesize and investigate some of the previously suggested catalysts in the reaction of secondary alcohols with butyraldehyde.

First, we intended to synthesize analogues of the catalysts reported by Li et al.[32] and examine them in the reaction of butyraldehyde with 2-butanol (2-BuOH) or 2,4-pentanediol. The target ionic compounds were the derivatives of aromatic *N*-heterocycles and thionyl chloride (Figure 1A). The choice of such unusual catalysts with an SOCl group and a labile N−S bond[33−35] seemed quite reasonable because the S atom has a

**Received:** March 11, 2015
**Revised:** April 19, 2015
**Published:** April 20, 2015





DOI: 10.1021/acs.jpca.5b02102
J. Phys. Chem. A 2015, 119, 4108−4117

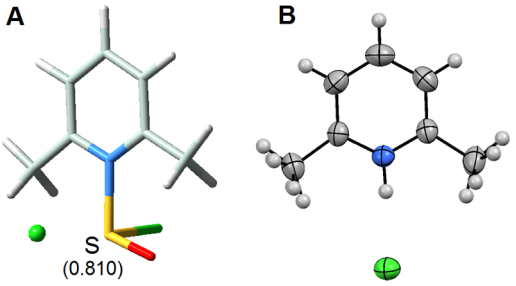


**Figure 1.** (A) Desired salt analog of functional ionic liquid described by Li et al.[32] The charge on the S atom is indicated in parentheses (Mulliken). (B) The X-ray crystal structure of 2,6-dimethylpyridine hydrochloride (**12**). Atomic displacement parameters are drawn at 50% probability level.

relatively high positive charge density and thus is expected to act as a Lewis acid.

However, instead of the desired catalyst, the molecular structure of the product was established as 2,6-dimethylpyridine hydrochloride (**12** in Table 1) from the single-crystal X-ray diffraction analysis (Figure 1B). It was later found that this simple organic salt was catalytically active toward the acetalization of 2-BuOH and 2,4-pentanediol with butyraldehyde. Therefore, we decided to synthesize a series of related organic salts, from the corresponding substituted pyridines, for use as catalysts for the acetalization reaction (for the usage of protic pyridinium salts as catalysts, see refs 36−41). 2-Propanol (*i*-PrOH), 2-BuOH, and 2,4-pentanediol were chosen as the substrates for studying the acetalization reaction in the presence of the obtained organic salts.

**Aims of the Study.** First, the efficiencies of the catalysts were to be investigated. In this study, we wanted to concentrate on the kinetics of the acetalization reactions carried out under the same conditions rather than on the yield of the final product.[42] The use of computational tools could dramatically reduce the number of compounds to be synthesized and tested.[43] Therefore, the second goal was to establish whether the activities of the catalysts correlated with their geometric or electronic characteristics computed with quantum chemical methods, and to use the results for the *in silico* design of novel highly efficient catalysts in the future. The final goal was to elucidate features of the hydrogen bond-assisted mechanism of the acetalization reaction catalyzed by the synthesized organic salts.

## EXPERIMENTAL AND THEORETICAL METHODS

**Kinetics Experiments.** *Acetalization of 2,4-Pentanediol with Butyraldehyde.* A 10 mL round-bottom flask containing a stir bar was charged with DMSO (6.0 g), 2,4-pentanediol (0.578 g, 5.5 mmol), butyraldehyde (0.5 mL, 0.4 g, 5.5 mmol), and toluene (internal standard, 10 mg, 0.1 mmol). The resultant mixture was thermostated at 60 °C for at least 15 min. After establishing temperature equilibrium, a small aliquot of the obtained mixture was sampled using a syringe (~10 μL) and subjected to GC analysis to verify the absence of the reaction and to establish the zero point for subsequent kinetics. Next, 0.27 mmol (0.05 equiv) of a catalyst was added as a single portion. The reaction progress was monitored by GC, for which small aliquots were sampled using a syringe at definite time intervals and immediately subjected to GC analysis.

The effective rate constants were calculated using eq 1, as described in our previous papers:[44,45]

**Table 1. Catalytic Activity of Various Organic Salts toward Acetalization of Secondary Alcohols**

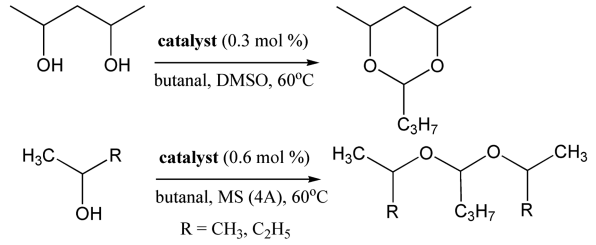


**Catalysts**

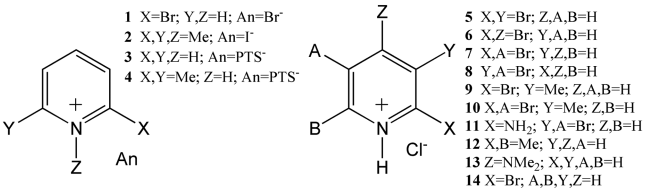


| entry | catalyst | loading, mol % | substrate | $k_{eff} \times 10^4$ l/mol sec |
|---|---|---|---|---|
| 1 | none | – | 2,4-pdl[a] | – |
| 2 | **1** | 0.3 | 2,4-pdl | 112.0 |
| 3 | **7** | 0.3 | 2,4-pdl | 99.0 |
| 4 | PTSA | 0.3 | 2,4-pdl | 97.7 |
| 5 | **9** | 0.3 | 2,4-pdl | 89.8 |
| 6 | **6** | 0.3 | 2,4-pdl | 89.0 |
| 7 | **5** | 0.3 | 2,4-pdl | 77.0 |
| 8 | **11** | 0.3 | 2,4pdl | 56.3 |
| 9 | **8** | 0.3 | 2,4-pdl | 36.0 |
| 10 | **10** | 0.3 | 2,4-pdl | 22.0 |
| 11 | **3** | 0.3 | 2,4-pdl | 16.1 |
| 12 | **4** | 0.3 | 2,4-pdl | 6.8 |
| 13 | **12** | 0.3 | 2,4-pdl | 5.2 |
| 14 | **13** | 0.3 | 2,4-pdl | 3.6 |
| 15 | **15**[b] | 0.3 | 2,4-pdl | 0.8 |
| 16 | **2** | 0.3 | 2,4-pdl | 0.8 |
| 17 | **5** | 0.6 | *i*-PrOH | 1.0 |
| 18 | **9** | 0.6 | *i*-PrOH | 0.69 |
| 19 | **1** | 0.6 | *i*-PrOH | 0.67 |
| 20 | **14** | 0.6 | *i*-PrOH | 0.63 |
| 21 | **11** | 0.6 | *i*-PrOH | 0.56 |
| 22 | PTSA | 0.6 | *i*-PrOH | 0.53 |
| 23 | **3** | 0.6 | *i*-PrOH | 0.43 |
| 24 | **4** | 0.6 | *i*-PrOH | 0.30 |
| 25 | HCl | 0.6 | *i*-PrOH | 0.16 |
| 26 | **12** | 0.6 | *i*-PrOH | 0.13 |
| 27 | **5** | 0.6 | 2-BuOH | 0.62 |
| 28 | **9** | 0.6 | 2-BuOH | 0.59 |
| 29 | **1** | 0.6 | 2-BuOH | 0.53 |
| 30 | **14** | 0.6 | 2-BuOH | 0.50 |
| 31 | PTSA | 0.6 | 2-BuOH | 0.10 |
| 32 | **4** | 0.6 | 2-BuOH | 0.10 |
| 33 | **12** | 0.6 | 2-BuOH | 0.04 |
| 34 | **13** | 0.6 | 2-BuOH | 0.02 |
| 35 | **5** | 0.3 | 2-BuOH | 0.25 |

[a]2,4-Pentanediol. [b]2-Chloroethyldimethylamine hydrochloride.

$$kt = \frac{1}{(c_{alc}^{\ 0} - c_a^{\ 0})} \ln\left(\frac{1 - \alpha_{alc}}{1 - \alpha_a}\right) \quad (1)$$

where $c_{alc}^{\ 0}$ is the initial alcohol concentration (M); $c_a^{\ 0}$ is the initial aldehyde concentration (M); $\alpha_a = (c_a^{\ 0} - c_a)/c_a^{\ 0}$ is the



DOI: 10.1021/acs.jpca.5b02102
J. Phys. Chem. A 2015, 119, 4108−4117

amount of aldehyde consumed; and $\alpha_{alc} = (c_{alc}^0 - c_{alc})/c_{alc}^0$ is the amount of hydroxyl converted. The values of $kt$, calculated from eq 1, were plotted against reaction time $t$. For all experiments, linear plots were obtained, and the effective rate constant $k_{eff}$ was calculated from the slope of each line.

*Acetalization of 2-Propanol and 2-Butanol with Butyraldehyde.* First, 10 mL round-bottom flask containing a stir bar was charged with alcohol (55 mmol), butyraldehyde (1 mL, 0.8 g, 11 mmol, 0.2 equiv), toluene (internal standard, 10 mg, 0.1 mmol), and 1 g of 4 Å MS. The resultant mixture was thermostated at 60 °C for at least 15 min. After that, 0.41 mmol of a catalyst was added as a single portion. The reaction progress was monitored by GC. Sampling procedures and calculations were analogous to those described above for the acetalization of 2,4-pentanediol.

**Computational Details.** All quantum mechanics calculations were performed using the Gaussian 03 program.[46] All geometry parameters of the studied systems were fully relaxed by searching for the energy minimum. DFT functionals employed in this study were hybrid generalized gradient approximation (GGA) B3LYP[47−49] and hybrid meta-GGA M06-HF.[50] B3LYP functional with the 6-31+G(d,p) basis set was used for ground-state calculations. A preliminary optimization procedure with the B3LYP/3-21G* level of theory was conducted in some cases. Previously, it was demonstrated that some hybrid density functionals such as B3LYP are not recommended for locating transition states due to errors in geometry associated in part with the underestimation of barrier height.[51] It was also stated that the commonly used 6-31+G(d,p) basis set is not sufficient for the best performance attainable with DFT methods, and a minimally augmented triple-$\zeta$ basis set was recommended.[51] Thus, for transition-state calculations, we used a combination of recommended hybrid meta-GGA M06-HF with the 6-311++G(d,p) basis set. A relaxed potential energy scan was employed prior to transition-state calculations. This approach was used to find the geometry of the complex with the maximum energy close to the transition-state structure. The O−H or N−H bond length was used as scanning variables. The M06-HF/6-311++G(d,p) method was also applied for the ground-state calculations of the pretransition-state complexes together with a combination of B3LYP and a 6-31+G(d,p) basis set. Individual pyridines and appropriate organic salts were optimized both in gas phase and by a condensed-phase simulation using a conductor-like polarizable continuum model[52,53] with DMSO as the solvent ($\varepsilon$ = 46.7). Hemiacetal-containing complexes were optimized by a condensed-phase simulation with ethanol solvent cavity ($\varepsilon$ = 24.6) using the integral equation formalism variant of the polarizable continuum model,[54,55] as implemented in Gaussian 03. Vibrational frequency calculations were conducted to confirm the transition states and local minima obtained and to determine zero-point vibrational energies and thermal corrections to the Gibbs free energies. Zero-point energies and thermal corrections to the energy at 298 K were included in the energy-barrier determination. The application of the natural bond orbital (NBO) analysis applied in this study has been described by Weinhold et al.[56−58] The mathematical and historical background of NBO methods can be found elsewhere.[59] On the basis of the NBO conception, hydrogen bond strength was determined as delocalization energy (e.g., electron transfer from donor to acceptor orbital) by the second-order perturbation theory. Thus, for each donor NBO ($i$) and acceptor NBO ($j$), the stabilization energy $E_{(2)}$ is estimated as follows:

$$E_{(2)} = E_{ij} = q_i \frac{F(i,j)^2}{\varepsilon_j - \varepsilon_i} \quad (2)$$

where $q_i$ is the donor orbital occupancy, $\varepsilon_i$ and $\varepsilon_j$ are orbital energies, and F($i$,$j$) is the off-diagonal NBO Fock matrix element. In this study, charges were calculated via natural population analysis (NPA)[57] and Mulliken population analysis.[60−63] NPA charge assignments were found to exhibit excellent numerical stability with respect to variations of basis extension and wave function form, as well as a gratifying agreement with empirical structure−function relationships and other well-known measures of charge distribution in physical organic chemistry.[58,64] Topological properties of the electron density were characterized using the "atoms in molecules" (AIM) methodology.[65,66] Bond critical points (BCPs) were located as extrema in the electron density where the gradient vector vanishes. This method has already been successfully employed to study noncovalent interactions such as conventional hydrogen bonds[67−69] and dihydrogen bonds.[70] Therefore, in this study, we used the BCP paradigm to verify H-bond formation.

## RESULTS AND DISCUSSION

**Kinetics of Acetal Formation.** In order to determine the relationships between the structures of the pyridinium-based ionic compounds **1**−**14** (Table 1) and their catalytic activity, a series of kinetic experiments were carried out. The formation of cyclic butyral was studied primarily, and 2,4-pentanediol was reacted with butyraldehyde at 60 °C in DMSO. As expected, no reaction was observed in the absence of additive (Table 1, entry 1). *N*-methyllutidinium iodide (**2**) and simple ammonium salt (**15**) showed the lowest (almost negligible) catalytic activity among the catalysts. Although 4-dimethylaminopyridine hydrochloride **13** and two derivatives of 2,6-dimethylpyridine (i.e., hydrochloride **12** and *p*-toluenesulfonate **4**) showed some activity, these were not sufficient for our study.

The acetalization reaction with 2,4-pentanediol is well-known to proceed with relatively high rates when catalyzed by inorganic (HCl) or organic (PTSA) Brönsted acids.[44,45] While, compounds **5**, **6**, and **9** showed high catalytic activity, compounds **7** and **1** showed better catalytic activity than the commonly employed PTSA. Next, the activities of various catalysts were investigated in the acetalization of butyraldehyde with *i*-PrOH and 2-BuOH. As shown in Table 1, catalysts **5**, **9**, **1**, and **14** were found to be the most efficient, whereas catalysts **12**, **3**, and **4** were the least efficient in the reactions with both the alcohols. Remarkably, simple protic pyridinium salts **1**, **5**, **9**, and **14** (and even **11**, see Table 1, entry 21) were capable of outperforming the strong acidic catalysts such as HCl and PTSA in these reactions (Figure 2).

One of the most impressive results was the extent of the observed catalytic activity. On the basis of the rate constant values, catalyst **5** was nearly two times more efficient than PTSA in the reaction with *i*-PrOH and more than six times more efficient than HCl and PTSA in the reaction with *i*-PrOH and 2-BuOH, respectively. Interestingly, the effect of more complex catalyst **11** was found to be marginal as it showed slightly better activity than PTSA in the reaction of *i*-PrOH with butyraldehyde; however, it showed lower activity


DOI: 10.1021/acs.jpca.5b02102
J. Phys. Chem. A 2015, 119, 4108−4117

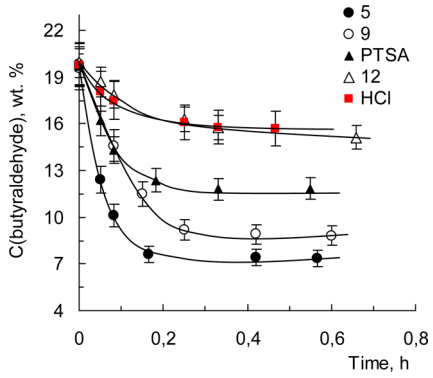


**Figure 2.** Butyraldehyde consumption, as a function of time, for acetalization of *i*-PrOH at 60 °C with various catalysts. [Cat] = 0.6 mol %.

compared to PTSA for the reaction of 2,4-pentanediol with butyraldehyde.

**Preliminary Structure–Activity Correlations for the Tested Catalysts Studied by X-ray, FTIR, and DFT Methods.** To support the kinetics experiments, the electronic and geometric characteristics of the catalysts and starting pyridines were computed at the B3LYP/6-31+G(d,p) level of theory. We were interested to determine whether the electronic and geometric characteristics of the organic salts correlated with the obtained $k_{eff}$ values. The results of the X-ray experiments and the data provided by several other studies[71−73] clearly showed that the acidic proton was located on the nitrogen of the heterocycle, indicating that the protonation and hence the N−H bond formation had taken place. Initially, it was established that the geometries calculated in solvent (DMSO) using the CPCM solvation model were close to the experimental geometries, whereas those calculated in the gas phase did not match the obtained X-ray results (Figure 3 and

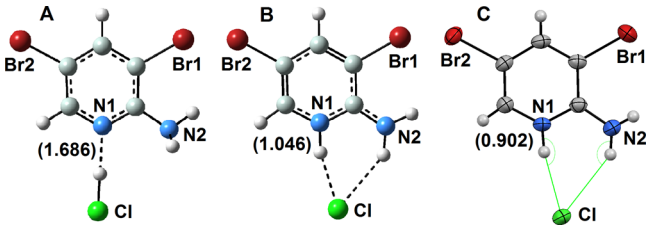


**Figure 3.** Geometries of catalyst **11**. (A) optimized in a gas phase at B3LYP/6-31+G(d,p) level of theory; (B) optimized in DMSO (CPCM solvation model) at the B3LYP/6-31+G(d,p) level of theory; (C) The X-ray crystal structure of organic salt. Atomic displacement parameters are drawn at the 50% probability level. Hydrogen bonds are shown by dashed lines.

Table S14 of the Supporting Information). Therefore, the following discussion is based on the results obtained for the molecules calculated under the liquid phase approximation.

Figure 4 shows the relationships between the N−H bond lengths of the protic pyridinium salts and the charges on the ring nitrogen of the appropriate bases as well as the dependence between the N−H bond lengths and the determined effective rate constants ($k_{eff}$). In both cases, fine correlations were observed that allowed us to conclude that the efficiency of the synthesized catalysts depends on the Lewis basicity of the pyridine substrate.

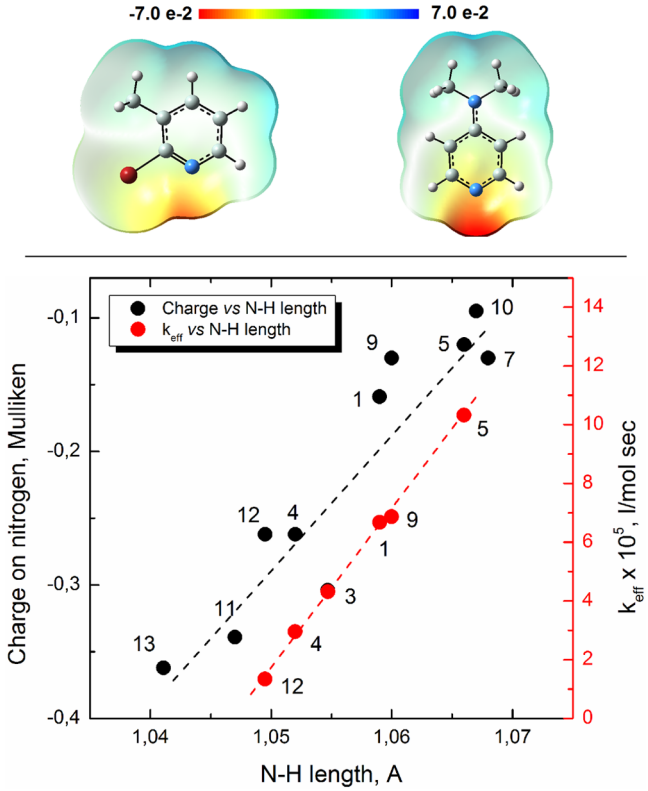


**Figure 4.** Top: Calculated electrostatic potential of precursors for catalysts 9 and 13. Units of color scale are in atomic units. Bottom: correlations of N−H distances (Å) in catalysts with charges on ring nitrogen (Mulliken) of precursors and effective rate constant ($k_{eff}$) calculated for acetalization of *i*-PrOH with butyraldehyde at 60 °C (red circles).

It was expected that the N−H bond distance, and hence the basicity of the former substrate as shown in Figure 4 by the charge on nitrogen, would reflect the lability and therefore the activity of the acidic proton in the acetalization reaction (e.g., in the reaction of 2,4-pentanediol with butyraldehyde in DMSO). Due to the relatively high electron density, the ring nitrogen binds strongly to the proton, thus making the N−H bond shorter and the proton less labile, thereby increasing the N−H stretching frequency ($\nu_{NH}$) in the experimental IR spectra.[74,75] The $\nu_{NH}$ of some pyridinium salts in DMSO-$d_6$ are plotted against both the charges on the ring nitrogen and $k_{eff}$ values (as shown in Figure 5). The positions of the $\nu_{NH}$ bands in the IR spectra of the organic salts in the liquid phase correlate with the Lewis basicities of the pyridines and simultaneously fit well to the calculated $k_{eff}$ values. The experimental and theoretical data confirm the above conclusion that the efficiencies of the protic pyridinium catalysts toward acetalization of the secondary alcohols depend primarily on the relative electronegativities on the ring nitrogen atoms, or in other words, on the basicities of the starting pyridines. In line with this concept, a decrease in the electron density around the ring nitrogen, which is usually achieved by introducing either electron-withdrawing groups (EWGs) or combining EWGs and electron-donating groups (EDGs) at certain positions of the pyridinium ring, increases the catalytic activity of the organic salt.

**Hydrogen Bond Orbital Interactions and Structure–Activity Correlations in Pretransition-State Complexes.** In general, the trends in the catalytic activities of the synthesized organic salts were the same for both cyclic and



DOI: 10.1021/acs.jpca.5b02102
J. Phys. Chem. A 2015, 119, 4108−4117

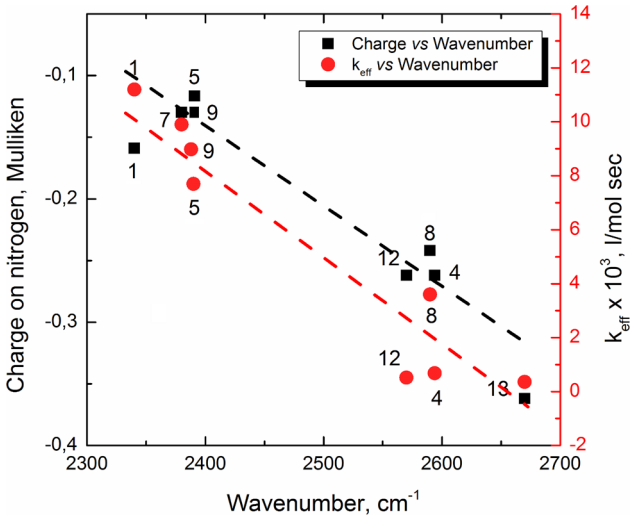


**Figure 5.** Plots of wavenumbers ($cm^{-1}$) correspond to N−H stretching mode in experimental IR spectra of various catalysts in DMSO-$d_6$, as functions of charge on ring nitrogen (Mulliken) of precursors and effective rate constant ($k_{eff}$) calculated for acetalization of 2,4-pentanediol with butyraldehyde in DMSO at 60 °C (red ●).

acyclic acetalization; for instance, in both the cases, catalysts **4**, **12**, and **13** were found to be much less active than catalysts **1**, **5**, **9**, and **14**. However, several important differences were observed between cyclic and acyclic acetal formation. The $k_{eff}$ values obtained for the acetalization of both *i*-PrOH and 2-BuOH were almost identical. In contrast, the analogous values were approximately 2 orders of magnitude higher in the acetalization of 2,4-pentanediol. These results confirmed that hemiacetal stabilization and subsequent transformation steps are the most difficult (thermodynamically unfavorable) and, therefore, rate determining.[17−19] Some organic salts were much more reactive toward the acetalization of *i*-PrOH and 2-BuOH than that of 2,4-pentanediol in comparison to classic Brönsted acids (PTSA and HCl, see Table 1). This fact could not be explained by the increased proton lability (acidity) or simple charge distribution in the precursors as described in a previous section. The observed effect could be explained by the stabilization of the hemiacetal intermediate with the protonated pyridines by H-bonding similar to the stabilization in chemzyme catalysis. H-bond parameters are known to crucially affect the reactivity of functional groups (for example, OH-groups[44,45,58]). H-bond formation leads to changes in electrostatic and orbital structures of the molecules involved. With an increase in H-bond strength, these changes also become more pronounced. The effect of intermolecular H-bonding on the rate coefficients for proton transfer will be considered first in this section by calculated pretransition-state complexes formed between the catalyst and hemiacetal molecule. We start our investigation with the characterization of the appropriate H-bonds. First, several criteria such as N−H bond length, distance between heavy atoms, H-bond length, and linearity, which typically define H-bond geometry, were used to establish H-bond formation in the complexes (for more details, please see ref 45). The H-bond critical point is a specific point between the proton donor and acceptor, where the electron density gradient is zero; it provides essential evidence for H-bond existence.[76,77] The calculated complexes with critical points (given as purple dots) for selective complexes are shown in Figure 6 and Figure S3 of the Supporting Information.

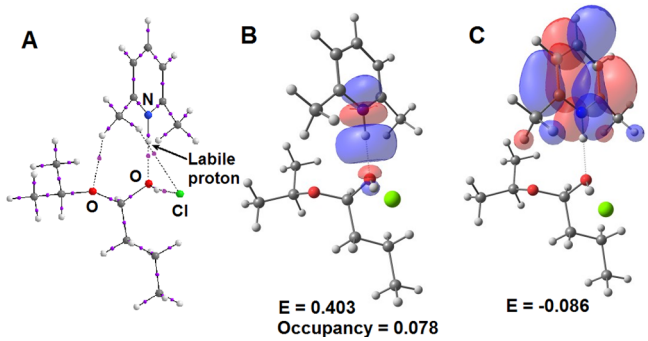


**Figure 6.** (A) Bond critical points (purple dots), (B) $\sigma^*_{NH}$ NBO, and (C) LUMO for the optimized pretransition-state complex of **12** and hemiacetal molecule. Orbital energies ($E$) are given in atomic units; occupancy is given in electrons (e).

It was found that all the complexes considered had a specific N−H···O hydrogen bond. To evaluate H-bond strength, typically, H-bond energy is calculated as the difference between the total energy of any considered complex and the sum of the energies of individual units (molecules) of this complex.[78] However, this method is only valid for relatively simple systems in which the considered H-bonding is the only dominant intermolecular interaction. As seen in Figure 6 and Figure S3 of the Supporting Information, various noncovalent interactions were established for the considered pretransition-state complexes; hence, the above-mentioned approach is not applicable. On the other hand, the highest occupied molecular orbital (HOMO) and lowest unoccupied molecular orbital (LUMO) are known to be very important parameters for determining the stabilities and reactivities of molecules or their complexes.[79−82] The HOMO energy characterizes the electron-donating ability; in contrast, the LUMO energy characterizes the electron-accepting ability, and the gap between them is an important stability index known to correlate with H-bond strength. However, this approach should be used with caution, due to the fact that even for the moderately complex molecular systems, MOs (frontier, in particular) have a complicated shape and are seen to be delocalized through various NAO-based localized sets (contain mixtures of Lewis and non-Lewis NBO orbitals). For example, considering the complex with catalyst **12** depicted in Figure 6, from our calculations, $LUMO_{12}$ was approximately expressed in LCNBO-MO form as follows: $LUMO_{12} = 0.167\pi_{NC} - 0.572\pi^*_{NC} - 0.404\pi_{CC} - 0.197n_C$. As can be seen, $LUMO_{12}$ is a complex hybrid, and the prime composition of this orbital does not contain $\sigma^*_{NH}$ antibonding or $n^*_H$ (antibonding lone pair denoted by LP* in NBO analysis) of the appropriate acidic proton that appears to be acceptor-type NBOs and are intuitively expected to comprise the LUMO. Hence, the energy of $LUMO_{12}$ does not reflect the electrophilic properties of the molecule associated with the acidic proton (H-activity). Consequently, one cannot consider the frontier MO approach to be correct for the evaluation of H-bond strength and chemical activities of the discussed reactive sites. On the contrary, the localized character of the NBO serves as an effective tool for analyzing these features of molecular systems. To determine the strength of a specific H-bond, we turned to the second-order perturbation theory of NBO donor−acceptor interactions, given by $E_{(2)}$. This parameter expressed the universal quantum mechanical paradigm for energetically stabilizing the superposition of occupied and unoccupied localized orbitals (occupied $n_O$ lone pair on


DOI: 10.1021/acs.jpca.5b02102
J. Phys. Chem. A 2015, 119, 4108−4117

hemiacetal OH oxygen with an unoccupied $\sigma^*_{NH}$ antibonding NBO on protonated pyridine in O:···HN alignment in our case).[58] Thus, a robust intermolecular $n_O \rightarrow \sigma^*_{NH}$ donor–acceptor interaction stabilizes the appropriate complex, and the larger $E_{(2)}$ value the more intensive the interaction (H-bond) and the greater the extent of stabilization. As seen in Figure 7,

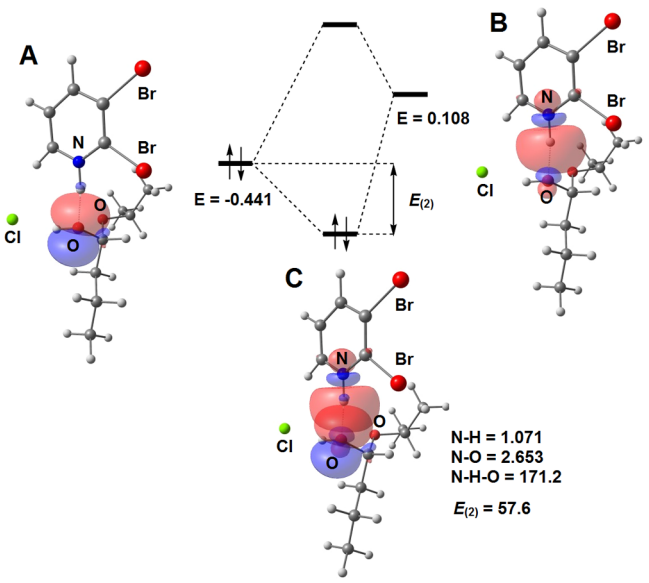


**Figure 7.** NBO (A) donor–(B) acceptor interaction diagram for H-bonded pretransition-state complex of **5** and hemiacetal molecule. Second-order stabilization energy ($E_{(2)}$) is in kcal/mol, orbital energies ($E$) are in atomic units, and bond distances in Angstroms.

donor and acceptor NBOs of the complex with catalyst **5** (analogous results were obtained for the systems with other catalysts) were found to be aligned appropriately for near-maximum intermolecular overlap, which explains the relatively high values of $E_{(2)}$ (Table 2).

**Table 2. M06-HF/6-311++G(d,p) Charges (NPA and Mulliken) on Transferred Proton, And Stabilization Energy $E_{(2)}$ for the Optimized Pretransition-State Complexes with Various Organic Salts**

| catalyst | NPA charges | Mulliken charges | $E_{(2)}$, kcal/mol |
|---|---|---|---|
| **5** | 0.503 | 0.460 | 57.63 |
| **1** | 0.502 | 0.456 | 38.26 |
| **14** | 0.501 | 0.455 | 37.68 |
| **9** | 0.501 | 0.452 | 37.65 |
| **11** | 0.495 | 0.436 | 30.39 |
| **12** | 0.488 | 0.416 | 26.08 |

Correlation plots, shown in Figure 8A, provide evidence that the intermolecular H-bond ($n_O \rightarrow \sigma^*_{NH}$ delocalization) is responsible for proton transfer from pyridine to the hemiacetal molecule as the experimental rate constant increases with increasing $E_{(2)}$. The stronger the H-bond (higher $E_{(2)}$ values), the more effective the corresponding catalyst.

In contrast to the normal $n_O \rightarrow \sigma^*_{NH}$ donor–acceptor interaction that was found in nearly all catalytic systems, the complex with 2,3-dibromopyridine hydrochloride (catalyst **5**) displayed an $n_O \rightarrow n^*_H$ interaction, which appeared to be significantly stronger than the $n_O \rightarrow \sigma^*_{NH}$ one ($E_{(2)nO\rightarrow n^*H}$ = 57.6 kcal mol$^{-1}$). As discussed previously by Weinhold et al.,[58] H-bonding in this case passes seamlessly into the covalent bonding regime as the proton is "half-transferred" from one Lewis base to the other. The "half-transferred" form of the proton is supported by the fact that no $\sigma^*_{NH}$ antibonding orbital exists in the pretransition-state complex of **5** with the hemiacetal, which in turn leads to the low activation energy of protonation (discussed in the next section). The calculated natural charges also conformed to the picture of the increasing rate constant with increasing H-bond strength as the obtained charge versus $k_{eff}$ plot (Figure 8B) exhibited the same trend. The illustrated correlations $E_{(2)}$ versus $k_{eff}$ and charge versus $k_{eff}$ confirm the significant role of H-bond formation between catalyst and substrate at the critical stage of acetalization and explains the superiority of some catalysts (especially 2,3-dibromopyridine hydrochloride) over convenient Brönsted acids as well as over the other catalysts tested for both cyclic and acyclic acetalization.

**Transition State for Proton Transfer from Pyridine to Hemiacetal Molecule.** According to Weinhold, H-bonding is essentially a partial proton-transfer reaction especially for strong interactions.[59] Hence, the ionic-resonance mnemonic, which usually describes the reactant → product process, suggests the relationship to the degree of completion of the discussed proton-transfer reaction (A–H···:B → [A:···H···:B]‡ → A:$^-$···H–B$^+$). In this section, we examine the proton-transfer reaction between three organic catalysts (**5** and **14** with high catalytic activity and **12** with low catalytic activity) and the hemiacetal molecule. The pretransition-state complexes of these catalysts have been discussed in a previous section. According to the calculations, the acceptor orbitals of **12** and **14** involved in H-bond formation were the unoccupied $\sigma^*_{NH}$ antibonding NBOs. Transition-state calculations revealed that the acceptor orbital for these two catalysts changed from $\sigma^*_{NH}$ to the antibonding lone pair NBO $n^*_H$; hence, the transferred proton could be considered as a separate unit bonded covalently neither to the pyridine nitrogen nor to the hemiacetal oxygen, as shown in Figure 9.

In contrast to catalysts **12** and **14**, the acceptor orbital of **5** has already been presented in a form of $n^*_H$; thus, only marginal perturbation (much weaker energetically than that for the $\sigma^*_{NH} \rightarrow n^*_H$ transformation as can be seen from Figure 10) is sufficient to transfer the proton from the pretransition-state complex to the transition state. As we have already stated in the case of the considered reaction, HOMO/LUMO energies are not informative for describing the orbital features of the reaction. Thus, we focused on the NBO localized on the donor (lone pair of the hemiacetal oxygen) and acceptor localized on the acidic proton. As shown in Figure 10, the low perturbation of both the $n_O$ orbital ($\Delta En_O$ = 0.060 au) and $n^*_H$ orbital ($\Delta En^*_H$ = 0.055 au) for the complex with catalyst **5** as compared with other complexes ($\Delta E_{nO}$ = 0.062 au, $\Delta E_{\sigma^*NH\rightarrow n^*H}$ = 0.321 au, for the complex with **14** and $\Delta E_{nO}$ = 0.108 au, $\Delta E_{\sigma^*NH\rightarrow n^*H}$ = 0.333 au, for the complex with the least-efficient catalyst **12**) leads to the lowest energy gap between the occupied and unoccupied NBO, which is also in agreement with the results of kinetic experiments.

By observing the changes in the occupancy of the transferred proton, one could note that this parameter dramatically changed for all but for **5**. Thus, the occupancy of the discussed antibonding orbital in the system with **12** changed from 0.078 e (pretransition complex) to 0.510 e (transition state). The appropriate change in the system with **14** was smaller (from 0.098 to 0.504 e), albeit still larg as compared with the shift in


DOI: 10.1021/acs.jpca.5b02102
J. Phys. Chem. A 2015, 119, 4108–4117

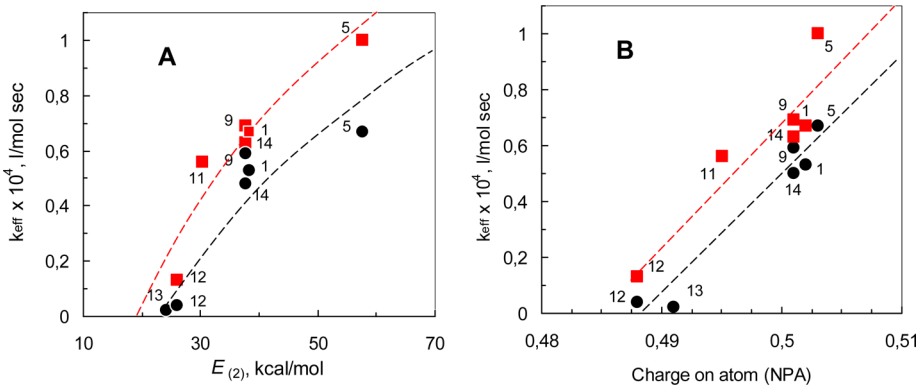


**Figure 8.** Correlations of (A) second-order stabilization energy ($E_{(2)}$) and (B) NPA charges on transferred proton with effective rate constant ($k_{eff}$) calculated for acetalization of *i*-PrOH (red ■) and 2-BuOH (black ●) with butyraldehyde at 60 °C.

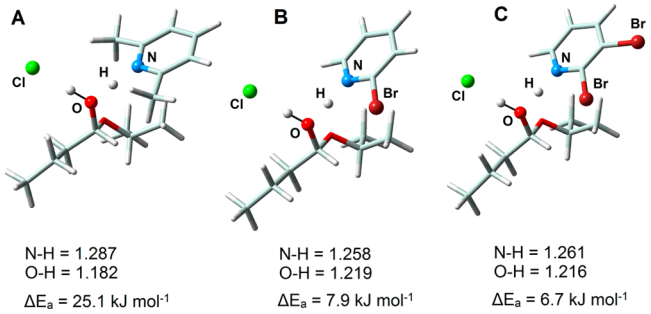


**Figure 9.** Optimized (M06-HF/6-311++G(d,p) transition-state structures for proton transfer from catalysts (A)**12**, (B) **14**, and (C) **5** to hemiacetal intermediate. Bond distances are in angstroms; $\Delta E_a$ corresponds to the energy barrier.

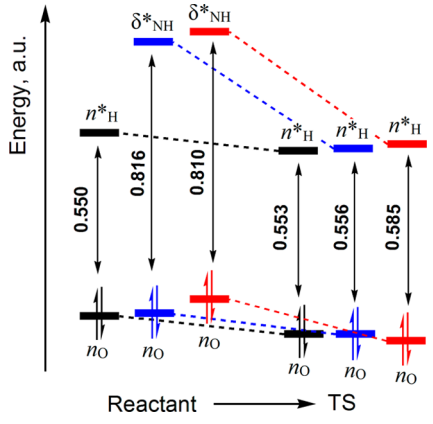


**Figure 10.** Transformations of the donor ($n_O$) and acceptor ($n^*_H$, $\sigma^*_{NH}$) orbitals in a course of the proton transfer between catalysts **5** (black), **14** (blue), **12** (red), and the hemiacetal molecule.

the complex with the highly active catalyst **5** (from 0.492 to 0.503 e). These observations supplemented with the results discussed in a previous section explain the fact that H-bond-catalyzed proton transfer for the system with 2,3-dibromopyridine hydrochloride (catalyst **5**) occurred with a relatively small energy barrier ($\Delta E_a$ = 6.7 kJ mol$^{-1}$) in contrast to other catalysts considered ($\Delta E_a$ = 25.1 for **12** and 7.9 kJ mol$^{-1}$ for **14**).

The obtained results support the idea that the hydrogen atom in a pretransition complex of the strong (effective) catalyst is electronically close to the "half-transferred" form, the origin of which is strong H-bonding that defines the activity of the tested catalyst.

## CONCLUSIONS

In summary, we demonstrated that pyridinium-based simple organic salts can act as efficient catalysts for the acetalization of secondary alcohols. The advantage of these catalysts, over traditional catalysts for this purpose, for example, is that strong Brönsted acids, such as PTSA and HCl, stem from the sufficient increase in the reaction rate under mild conditions. As a general trend, the presence of either electron-withdrawing groups or a combination of electron-withdrawing groups and electron-donating groups at certain positions of the pyridinium ring leads to increasing lability of the acidic proton, which makes the H-bond formed between the protic pyridinium salt and hemiacetal intermediate stronger. The interpretation of the H-bonded ground-state complexes for the strong catalysts (especially for 2,3-dibromopyridine hydrochloride) in terms of partial proton transfer was discussed. From the orbital and electronic viewpoints, H-bond strength correlates with the activity of the tested catalysts; thus, strong H-bonds facilitate appropriate proton transfer. Our investigations demonstrate that results of the pretransition-state (ground state) calculations conform to those of the kinetic experiments and are also in line with determined energy barriers. Thus, we have shown that for the described type of the reaction (proton transfer), one could use optimized pretransition-state complexes to search for potentially effective novel catalysts prior to the experiment. This approach avoids the use of more difficult and much more time-consuming transition-state calculations, which is of special importance for molecular systems of moderate and large complexity and is promising to be attractive for researchers in the field of artificial enzyme chemistry, which is often based on H-bond-assisted reactions.

## ASSOCIATED CONTENT

### Supporting Information

General considerations and additional experimental procedures, additional theoretical results, spectral data and CIF file for catalysts **1**, **11**, and **12**. The Supporting Information is available free of charge on the ACS Publications website at DOI: 10.1021/acs.jpca.5b02102.

## AUTHOR INFORMATION

### Corresponding Author

*E-mail: rumih@mail2k.ru.



DOI: 10.1021/acs.jpca.5b02102
J. Phys. Chem. A 2015, 119, 4108−4117

### Notes

The authors declare no competing financial interest.

## ■ ACKNOWLEDGMENTS

This work was financially supported by the Russian Foundation for Basic Research (project no. 14-03-31973).

## ■ REFERENCES

(1) Wang, Y.; Jiang, D.; Dai, L. Novel Brønsted Acidic Ionic Liquids Based on Benzimidazolium Cation: Synthesis and Catalyzed Acetalization of Aromatic Aldehydes with Diols. *Catal. Commun.* **2008**, *9*, 2475−2480.

(2) Dai, Y.; Li, B. D.; Quan, H. D.; Lu, C. X. $[Hmim]_3PW_{12}O_{40}$: A High-Efficient and Green Catalyst for the Acetalization of Carbonyl Compounds. *Chin. Chem. Lett.* **2010**, *21*, 678−681.

(3) Liang, X. Z.; Gao, S.; Chen, S.; Chen, W. P.; Wang, W. P.; Yang, J. G. Synthesis of a Novel Carbon Based Acid Catalyst and Its Catalytic Activity for the Acetalization and Ketalization. *Chin. J. Chem.* **2007**, *25*, 1795−1797.

(4) Liang, X.; Cheng, Y.; Qi, C. Polypyrrole Based Strong Acid Catalyst for Acetalization. *Solid State Sci.* **2011**, *13*, 1820−1824.

(5) Mehrjardi, M. F.; Ghanemi, K. Melamine Trisulfonic Acid Acetalization of Carbonyl Compounds under Solvent-Free Conditions. *Jordan J. Chem.* **2012**, *7*, 393−399.

(6) Li, D.; Shi, F.; Peng, G.; Guo, S.; Deng, Y. Application of Functional Ionic Liquids Possessing Two Adjacent Acid Sites for Acetalization of Aldehydes. *J. Org. Chem.* **2004**, *69*, 3582−3585.

(7) Wu, H. H.; Yang, F.; Cui, P.; Tang, J.; He, M. Y. An Efficient Procedure for Protection of Carbonyls in Brønsted Acidic Ionic Liquid [Hmim]BF4. *Tetrahedron Lett.* **2004**, *45*, 4963−4965.

(8) Narasaka, K.; Inoue, M.; Yamada, T.; Sugimori, J.; Iwasawa, N. Asymmetric Diels-Alder Reaction by the Use of a Chiral Titanium Catalyst with Molecular Sieves 4A. Remarkable Solvent Effect on the Enantioselectivity. *Chem. Lett.* **1987**, *16*, 2409−2412.

(9) Ruger, A. J.; Nieger, M.; Es-Sayed, M.; Brase, S. Novel 2,5-Disubstituted 1,3-Dioxanes and Oxazolidines as Potential Chemoprevention Agents and Building Blocks for Organic Synthesis. *Eur. J. Org. Chem.* **2010**, 3837−3846.

(10) Bi, L.; Zhao, M.; Gu, K.; Wang, C.; Ju, J.; Peng, S. Toward the Development of Chemoprevention Agents (III): Synthesis and Anti-Inflammatory Activities of a New Class of 5-Glycylamino-2-Substituted-Phenyl-1,3-Dioxacycloalkanes. *Bioorg. Med. Chem.* **2008**, *16*, 1764−1774.

(11) Li, X.; Zhao, M.; Tang, Y.-R.; Wang, C.; Zhang, Z.; Peng, S. *N*-[2-(5,5-Dimethyl-1,3-Dioxane-2-yl)ethyl]amino Acids: Their Synthesis, Anti-Inflammatory Evaluation and QSAR Analysis. *Eur. J. Med. Chem.* **2008**, *43*, 8−18.

(12) Gopinath, R.; Haque, S. J.; Patel, B. K. Tetrabutylammonium Tribromide (TBATB) as An Efficient Generator of HBr for an Efficient Chemoselective Reagent for Acetalization of Carbonyl Compounds. *J. Org. Chem.* **2002**, *67*, 5842−5845.

(13) Kotke, M.; Schreiner, P. R. Acid-Free, Organocatalytic Acetalization. *Tetrahedron* **2006**, *62*, 434−439.

(14) Augustine, J. K.; Bombrun, A.; Sauer, W. H. B.; Vijaykumar, P. Highly Efficient and Chemoselective Acetalization and Thioacetalization of Aldehydes Catalyzed by Propylphosphonic Anhydride (®T3P) at Room Temperature. *Tetrahedron Lett.* **2012**, *53*, 5030−5033.

(15) Mei, Y.; Bentley, P. A.; Du, J. NCS With Thiourea as Highly Efficient Catalysts for Acetalization of Aldehydes. *Tetrahedron Lett.* **2009**, *50*, 4199−4200.

(16) Zhu, Y. W.; Yi, W. B.; Cai, C. A Recyclable Fluorous Hydrazine-1,2-bis(carbothioate) with NCS as Efficient Catalysts for Acetalization of Aldehydes. *New J. Chem.* **2013**, *37*, 890−892.

(17) Nakamura, N.; Suzuki, K. Study on Ketalization Reaction of Poly(vinyl Alcohol) by Ketones. VIII. Kinetic Study on Acetalization and Ketalization Reactions of Poly(vinyl Alcohol). *J. Polym. Sci., Part A* **1996**, *34*, 3319−3328.

(18) Ogato, Y.; Okano, M.; Ganke, T. Kinetics of the Formation of the Formal of Polyvinyl Alcohol. *J. Am. Chem. Soc.* **1956**, *78*, 2962−2964.

(19) Kormanovskaya, G. N.; Vlodavets, I. N. Kinetics of the Homogeneous Interaction of Polyvinyl Alcohol with Formaldehyde in Aqueous Solutions. *Russ. Chem. Bull.* **1964**, *13*, 1661−1666.

(20) Lin, Y.; Zhao, A.; Tao, Y.; Ren, J.; Qu, X. Ionic Liquid as an Efficient Modulator on Artificial Enzyme System: Toward the Realization of High-Temperature Catalytic Reactions. *J. Am. Chem. Soc.* **2013**, *135*, 4207−4210.

(21) Lindback, E.; Zhou, Y.; Pedersen, C. M.; Bols, M. Artificial Enzymes Based on Cyclodextrin with Phenol as the Catalytic Group. *Tetrahedron Lett.* **2012**, *53*, 5023−5026.

(22) Ren, H.; Wulff, D. W. Direct Catalytic Asymmetric Amino-allylation of Aldehydes: Synergism of Chiral and Nonchiral Brønsted Acids. *J. Am. Chem. Soc.* **2011**, *133*, 5656−5659.

(23) Hu, G.; Gupta, A. K.; Huang, R. H.; Mukherjee, M.; Wulff, W. D. Substrate-Induced Covalent Assembly of a Chemzyme and Crystallographic Characterization of a Chemzyme−Substrate Complex. *J. Am. Chem. Soc.* **2010**, *132*, 14669−14675.

(24) Xiao, J.; Xu, F. X.; Lu, Y. P.; Loh, T. P. Chemzymes: A New Class of Structurally Rigid Tricyclic Amphibian Organocatalyst Inspired by Natural Product. *Org. Lett.* **2010**, *12*, 1220−1223.

(25) Zhang, Y.; Lu, Z.; Desai, A.; Wulff, W. D. Mapping the Active Site in a Chemzyme: Diversity in the *N*-Substituent in the Catalytic Asymmetric Aziridination of Imines. *Org. Lett.* **2008**, *10*, 5429−5432.

(26) Kim, J. H.; Coric, I.; Vellalath, S.; List, B. The Catalytic Asymmetric Acetalization. *Angew. Chem., Int. Ed.* **2013**, *52*, 4474−4477.

(27) Mahlau, M.; List, B. Asymmetric Counteranion-Directed Catalysis: Concept, Definition, and Applications. *Angew. Chem., Int. Ed.* **2013**, *52*, 518−533.

(28) Kniep, F.; Jungbauer, S. H.; Zhang, Q.; Walter, S. M.; Schindler, S.; Schnapperelle, I.; Herdtweck, E.; Huber, S. Organocatalysis by Neutral Multidentate Halogen-Bond Donors. *Angew. Chem., Int. Ed.* **2013**, *52*, 7028−7032.

(29) Holland, M. C.; Paul, S.; Schweizer, B.; Bergander, K.; Mück-Lichtenfeld, C.; Lakhdar, S.; Mayr, H.; Gilmour, R. Noncovalent Interactions in Organocatalysis: Modulating Conformational Diversity and Reactivity in the MacMillan Catalyst. *Angew. Chem., Int. Ed.* **2013**, *52*, 7967−7971.

(30) Beckendorf, S.; Asmus, S.; Mancheno, O. G. H-Donor Anion Acceptor Organocatalysis−the Ionic Electrophile Activation Approach. *ChemCatChem.* **2012**, *4*, 926−936.

(31) Procuranti, B.; Connon, S. J. Unexpected Catalysis: Aprotic Pyridinium Ions as Active and Recyclable Brønsted Acid Catalysts in Protic Media. *Org. Lett.* **2008**, *10*, 4935−4938.

(32) Li, D.; Shi, F.; Peng, J.; Guo, S.; Deng, Y. Application of Functional Ionic Liquids Possessing Two Adjacent Acid Sites for Acetalization of Aldehydes. *J. Org. Chem.* **2004**, *69*, 3582−3585.

(33) Xuan, J.; Li, B. J.; Feng, Z. J.; Sun, G. D.; Ma, H. H.; et al. Desulfonylation of Tosyl Amides through Catalytic Photoredox Cleavage of N−S Bond Under Visible-Light Irradiation. *Chem.—Asian J.* **2013**, *8*, 1090−1094.

(34) Paquette, L. A.; Dura, R. D.; Fosnaugh, N.; Stepanian, M. Direct Comparison of the Response of Bicyclic Sultam and Lactam Dienes to Photoexcitation. Concerning the Propensity of Differing Bond Types to Bridgehead Nitrogen for Homolytic Cleavage. *J. Org. Chem.* **2006**, *71*, 8438−8445.

(35) Piggott, A. M.; Karuso, P. Hydrolysis Rates of Alkyl and Aryl Sulfinamides: Evidence of General Acid Catalysis. *Tetrahedron lett.* **2007**, *48*, 7452−7455.

(36) Tajbakhsh, M.; Alinezhad, H.; Norouzi, M.; Baghery, S.; Akbari, M. Protic Pyridinium Ionic Liquid as a Green and Highly Efficient Catalyst for the Synthesis of Polyhydroquinoline Derivatives via Hantzsch Condensation in Water. *J. Mol. Liq.* **2013**, *177*, 44−48.

(37) Greaves, T. G.; Drummond, C. Protic Ionic Liquids: Properties and Applications. *Chem. Rev.* **2008**, *108*, 206−237.



DOI: 10.1021/acs.jpca.5b02102
*J. Phys. Chem. A* 2015, 119, 4108−4117

(38) Duan, Z.; Gu, Y.; Zhang, J.; Zhu, L.; Deng, Y. Protic Pyridinium Ionic Liquids: Synthesis, Acidity Determination and their Performances for Acid Catalysis. *J. Mol. Catal. A-Chem.* **2006**, *250*, 163−168.
(39) Chen, X.; Liu, R.; Xu, Y.; Zou, G. Tunable Protic Ionic Liquids as Solvent−Catalysts for Improved Synthesis of Multiply Substituted 1,2,4-Triazoles from Oxadiazoles and Organoamines. *Tetrahedron* **2012**, *68*, 4813−4819.
(40) Matsuo, J.; Hattori, Y.; Ishibashi, H. Brønsted Acid Catalyzed Asymmetric Reduction of Ketones and Acyl Silanes Using Chiral *anti*-Pentane-2,4-diol. *Org. Lett.* **2010**, *12*, 2294−2297.
(41) Wang, W.; Liu, H.; Xu, S.; Gao, Y. Esterification Catalysis by Pyridinium *p*-Toluenesulfonate Revisited—Modification with a Lipid Chain for Improved Activities and Selectivities. *Synth. Commun.* **2013**, *43*, 2906−2912.
(42) Meskens, F. A. J. Methods for the Preparation of Acetals from Alcohols or Oxiranes and Carbonyl Compounds. *Synthesis* **1981**, *7*, 501−522.
(43) Fanfrlik, J.; Bronowska, A. K.; Rezac, J.; Prenosil, O.; Konvalinka, J.; Hobza, P. A Reliable Docking/Scoring Scheme Based on the Semiempirical Quantum Mechanical PM6-DH2Method Accurately Covering Dispersion and H-Bonding: HIV-1 Protease with 22 Ligands. *J. Phys. Chem. B* **2010**, *114*, 12666−12678.
(44) Rumyantsev, M. S.; Gushchin, A. V.; Zelentsov, S. V. Effect of the Type of Hydrogen Bonding on the Reactivity of Hydroxyl Groups in the Acetalization of Poly(vinyl alcohol) with Butanal. *Polym. Sci. B* **2012**, *54*, 464−71.
(45) Rumyantsev, M.; Zelentsov, S. V.; Gushchin, A. V. Retardation Effect in Acetalization of Poly(vinyl alcohol) with Butyraldehyde. *Eur. Polym. J.* **2013**, *49*, 1698−1706.
(46) Gaussian 03, Revision B.03, Frisch, M. J.; Trucks, G. W.; Schlegel, H. B.; Scuseria, G. E.; Robb, M. A.; Cheeseman, J. R.; Scalmani, G.; Barone, V.; Mennucci, B.; Petersson, G. A. et al. Gaussian, Inc., Pittsburgh, PA, 2003.
(47) Lee, C.; Yang, W.; Parr, R. G. Development of the Colle-Salvetti Correlation-Energy Formula into a Functional of the Electron Density. *Phys. Rev. B* **1988**, *37*, 785−789.
(48) Adamo, C.; Barone, V. Toward Reliable Adiabatic Connection Models Free From Adjustable Parameters. *Chem. Phys. Lett.* **1997**, *274*, 242−250.
(49) Becke, A. D. Density-Functional Thermochemistry. V. Systematic Optimization of Exchange-Correlation Functional. *J. Chem. Phys.* **1997**, *107*, 8554−8560.
(50) Zhao, Y.; Truhlar, D. G. Density Functional for Spectroscopy: No Long-Range Self-Interaction Error, Good Performance for Rydberg and Charge-Transfer States, and Better Performance on Average than B3LYP for Ground States. *J. Phys. Chem. A* **2006**, *110*, 13126−13130.
(51) Xu, X.; Alecu, I. M.; Truhlar, D. G. How Well Can Modern Density Functionals Predict Internuclear Distances at Transition States? *J. Chem. Theory Comput.* **2011**, *7*, 1667−1676.
(52) Barone, V.; Cossi, M. Quantum Calculation of Molecular Energies and Energy Gradients in Solution by a Conductor Solvent Model. *J. Phys. Chem. A* **1998**, *102*, 1995−2001.
(53) Cossi, M.; Rega, N.; Scalmani, G.; Barone, V. Energies, Structures, and Electronic Properties of Molecules in Solution with the C-PCM Solvation Model. *J. Comput. Chem.* **2003**, *24*, 669−681.
(54) Miertuš, S.; Tomasi, J. Approximate Evaluations of the Electrostatic Free Energy and Internal Energy Changes in Solution Processes. *Chem. Phys.* **1982**, *65*, 239−245.
(55) Barone, V.; Cossi, M.; Tomasi, J. A New Definition of Cavities for the Computation of Solvation Free Energies by the Polarizable Continuum Model. *J. Chem. Phys.* **1997**, *107*, 3210−3221.
(56) Reed, A. E.; Weinhold, F. Natural Bond Orbital Analysis of Near-Hartree−Fock Water Dimer. *J. Chem. Phys.* **1983**, *78*, 4066−4073.
(57) Reed, A. E.; Weinstock, R. B.; Weinhold, F. Natural Population Analysis. *J. Chem. Phys.* **1985**, *83*, 735−746.
(58) Glendening, E. D.; Landis, C. R.; Weinhold, F. Natural Bond Orbital Methods. *WIREs Comput. Mol. Sci.* **2012**, *2*, 1−42.
(59) Weinhold, F.; Landis, C. R. *Valency and Bonding: A Natural Bond Orbital Donor-Acceptor Perspective*; Cambridge University Press: Cambridge, UK, 2005.
(60) Mulliken, R. S. Electronic Population Analysis on LCAO−MO Molecular Wave Functions. I. *J. Chem. Phys.* **1955**, *23*, 1833−1840.
(61) Mulliken, R. S. Electronic Population Analysis on LCAO−MO Molecular Wave Functions. II. Overlap Populations, Bond Orders, and Covalent Bond Energies. *J. Chem. Phys.* **1955**, *23*, 1841−1846.
(62) Mulliken, R. S. Electronic Population Analysis on LCAO-MO Molecular Wave Functions. III. Effects of Hybridization on Overlap and Gross AO Populations. *J. Chem. Phys.* **1955**, *23*, 2338−2342.
(63) Mulliken, R. S. Electronic Population Analysis on LCAO-MO Molecular Wave Functions. IV. Bonding and Antibonding in LCAO and Valence-Bond Theories. *J. Chem. Phys.* **1955**, *23*, 2343−2346.
(64) Gross, K. C.; Seybold, P. G. Substituent Effects on the Physical Properties and p*Ka* of Aniline. *Int. J. Quantum Chem.* **2000**, *80*, 1107−1115.
(65) Bader, R. F. W. *Atoms in Molecules: A Quantum Theory*; Oxford University Press: Oxford, UK, 1990.
(66) Stefanov, B. B.; Cioslowski, J. An Efficient Approach to Calculation of Zero-Flux Atomic Surfaces and Generation of Atomic Integration Data. *J. Comput. Chem.* **1995**, *16*, 1394−1404.
(67) Carroll, M. T.; Bader, R. F. W. An Analysis of the Hydrogen Bond in BASE-HF Complexes Using the Theory of Atoms in Molecules. *Mol. Phys.* **1988**, *65*, 695−722.
(68) Carroll, M. T.; Chang, C.; Bader, R. F. W. Prediction of the Structures of Hydrogen-Bonded Complexes Using the Laplacian of the Charge Density. *Mol. Phys.* **1988**, *63*, 387−405.
(69) Cheeseman, J. R.; Carroll, M. T.; Bader, R. F. W. The Mechanics of Hydrogen Bond Formation in Conjugated Systems. *Chem. Phys. Lett.* **1988**, *143*, 450−458.
(70) Popelier, P. L. A. Characterization of a Dihydrogen Bond on the Basis of the Electron Density. *J. Phys. Chem. A* **1998**, *102*, 1873−1878.
(71) Awwadi, F. F.; Willett, R. D.; Peterson, K. A.; Twamley, B. The Nature of Halogen···Halide Synthons: Theoretical and Crystallographic Studies. *J. Phys. Chem. A* **2007**, *111*, 2319−2328.
(72) Awwadi, F. F.; Willett, R. D.; Twamley, B. The Role of Charge Assisted Arylhalogen−Halide Ion Interactions in the Structures of the Dibromopyridinium Halide Salts. *J. Mol. Struct.* **2009**, *918*, 116−122.
(73) Chao, M.; Schempp, E.; Rosenstein, R. D. 4-Dimethylaminopyridine Hydrochloride Dehydrate. *Acta Cryst. B* **1977**, *33*, 1820−1823.
(74) Glazunov, V. P.; Odinokov, S. E. Infrared Spectra of Pyridinium Salts in Solution − II. Fermi Resonance and Structure of $\nu_{NH}$ Bands. *Spectrochim. Acta, Part A* **1982**, *38*, 409−415.
(75) Odinokov, S. E.; Mashkovsky, A. A.; Glazunov, V. P. Infrared Spectra of Pyridinium Salts in Solution − III. Associations of Pyridinium Salts with Bases. *Spectrochim. Acta, Part A* **1983**, *39*, 1065−1071.
(76) Lane, J. R.; Contreras-Garcia, J.; Piquemal, J.; Miller, B. J.; Kjaergaard, H. G. Are Bond Critical Points Really Critical for Hydrogen Bonding? *J. Chem. Theory Comput.* **2013**, *9*, 3263−3266.
(77) Snehanshu, P.; Kundu, T. K. Theoretical Study of Hydrogen Bond Formation in Trimethylene Glycol-Water Complex. *ISRN Phys. Chem.* **2012**, 1−12.
(78) Parthasarathi, R.; Subramanian, V.; Sathyamurthy, N. Hydrogen Bonding in Phenol, Water, and Phenol−Water Clusters. *J. Phys. Chem. A* **2005**, *109*, 843−850.
(79) Karnan, M.; Balachandran, V.; Murugan, M.; Murali, M. K.; Nataraj, A. Vibrational (FT-IR and FT-Raman) Spectra, NBO, HOMO−LUMO, Molecular Electrostatic Potential Surface and Computational Analysis of 4-(Trifluoromethyl)benzylbromide. *Spectrochim. Acta, Part A* **2013**, *116*, 84−95.
(80) Srivastava, A.; Tandon, P.; Jain, S.; Asthana, B. P. Antagonistic Properties of a Natural Product − Bicuculline with the Gamma-Aminobutyric Acid Receptor: Studied through Electrostatic Potential Mapping, Electronic and Vibrational Spectra Using *ab initio* and Density Functional Theory. *Spectrochim. Acta, Part A* **2011**, *84*, 144−155.


DOI: 10.1021/acs.jpca.5b02102
*J. Phys. Chem. A* 2015, 119, 4108−4117

(81) Vektariene, A. Insights into the Mechanism of the Benzoannelated Thieno[3,2-*b*]furan Halogenation. Importance of HOMO−HOMO Interaction. *J. Phys. Chem. A* **2013**, *117*, 8449−8458.
(82) Mebi, C. A. DFT Study on Structure, Electronic Properties, and Reactivity of *cis*-Isomers of $[(NC_5H_4\text{-}S)_2Fe(CO)_2]$. *J. Chem. Sci.* **2011**, *123*, 727−731.



DOI: 10.1021/acs.jpca.5b02102
*J. Phys. Chem. A* 2015, 119, 4108−4117